Heliyon 10 (2024) e32184

Contents lists available at ScienceDirect

Heliyon

journal homepage: www.cell.com/heliyon

Research article

Cation-induced morphological transitions and aggregation of thermoresponsive PNIPAM nanogels

Yuchen Zhu [a,b], Jiaxin Hou [a,b], Dominic M. Gray [c], Tom O. McDonald [a,b,c], Ahu Gümrah Dumanli [a,b,*]

[a] Department of Materials, The University of Manchester, Oxford Rd, Manchester, M13 9PL, UK
[b] Henry Royce Institute, The University of Manchester, Oxford Rd, Manchester, M13 9PL, UK
[c] Department of Chemistry, University of Liverpool, Crown Street, Liverpool, L69 7ZD, UK

ARTICLE INFO

Keywords:
PNIPAM nanogels
Colloidal stability
Cation induced morphology
Debye screening model
Zeta potential

ABSTRACT

Poly(*N*-isopropylacrylamide) (PNIPAM) nanogels are promising responsive colloidal particles that can be used in pharmaceutical applications as drug carriers. This work investigates the temperature-dependent morphological changes and agglomeration of PNIPAM nanogels in the presence of mono- and multi-valent cationic electrolytes. We described the deswelling, flocculation, thermal reversibility behaviour and aggregated morphology of PNIPAM nanogels over a range of electrolyte concentrations and temperatures revealing the critical transition points from stable suspension to spontaneous agglomeration. We demonstrated that the flocculating ability and the rate of aggregate formation follow the order of deswelling behaviour. Transmission electron microscopy and atomic force microscopy analysis revealed the presence of a shell-like layer with varying density in the multivalent electrolyte solutions when compared to those in aqueous medium. We identified a concentration threshold of the thermally induced reversible aggregation/dispersion for the PNIPAM nanogels in the presence of Na^+ and K^+ ions at 10 mM, for Mg^{2+} and Ca^{2+} ions at 1 mM and for Al^{3+} ions at 0.1 mM concentrations. Such concentration thresholds indicated the effective destabilization of the electrolyte system with multivalency following the Schulze–Hardy rule. Our findings were supported by applying a Debye screening model that accounts for the shielding effect of multivalent cationic electrolytes on these nanogel systems. Our experiments and the models confirmed the compression of the electric double layer as the valency and ionic strength increased, except for Al^{3+} at higher concentrations which seemed to disrupt the electrical double layer and cause reversal of zeta potential. Our work highlights the significant impact the presence of multivalent cations can impose on the stability and morphology of nanogels, and this understanding will help in designing responsive nanogel systems based on PNIPAM nanogels.

1. Introduction

Poly(*N*-isopropylacrylamide) (PNIPAM) nanogels are cross-linked polymer particles that exhibit a temperature-responsive transition at ~ 32 °C, known as the volume phase transition temperature (VPTT) [1]. These nanogels have received growing attention due

* Corresponding author. Department of Materials, The University of Manchester, Oxford Rd, Manchester, M13 9PL, UK.
E-mail address: ahugumrah.parry@manchester.ac.uk (A.G. Dumanli).

https://doi.org/10.1016/j.heliyon.2024.e32184
Received 22 November 2023; Received in revised form 9 May 2024; Accepted 29 May 2024
Available online 31 May 2024

to their VPTT being close to body temperature and their rapid phase transition [2–4]. Such temperature responsiveness of the PNIPAM nanogels has generated great interest in potential applications such as drug delivery [5–9], tissue engineering [10–12], and wound dressing [13,14].

The colloidal stability of PNIPAM nanogels is dependent on both steric repulsion and electrostatic repulsion, these types of stability result of the interplay between the solvated polymer chains on the surface and the initiator-derived anionic charges on the particles, respectively [15,16]. While the steric repulsion has a strong temperature dependency and will disappear as the nanogels deswell above the VPTT [17], in the presence of ions, the electrostatic repulsion also plays a critical role in the colloidal stability of the nanogel dispersion. Such electrostatic repulsion between colloids is demonstrated to be diminished by the increased ionic strengths [18]. Therefore, the nanogels are responsive to both temperature and ionic strength changes. Understanding such response with respect to these stimuli is therefore crucial in terms of designing smart nanogel systems with controlled agglomeration and dispersion states in complex biological environments.

There have been studies investigating the flocculation behaviour and VPTT of PNIPAM particles in the presence of cation- or anion-based electrolyte systems with respect to their valency (mono- and di-valency) [19–24]. The cation-based studies revealed that the flocculation of the nanogels was predominantly determined by the electrolyte species and their concentration [19] and their VPTT became broader and shifted to a lower temperature with increasing the electrolyte valency and concentration [20]. Additionally, Pastoor et al. reported that the phase behaviour of PNIPAM hydrogel was determined by the competing hydrophilic and hydrophobic forces, where cation solvation aided the stabilization [22]. Such power of facilitating the volume phase transition follow the order $Ca^{2+} < Mg^{2+} < Na^{+}$. In terms of the effects of anions, it has been shown that the flocculation behaviour correlates with the lyotropic series (Hofmeister series) [25,26]. Such that the solvating ions such as Cl^{-} had greater efficiency in deswelling than non-solvating (SCN^{-}) ions [27]. Lopez-Leon et al. further revealed the mechanism of Hofmeister effect on PNIPAM particles in their study, which focused on the investigation of the polymer network configuration and interfacial properties. They revealed the change in structure at the water interface around the PNIPAM chains and ionic adsorption-exclusion phenomena at the polymer surface in the presence of Hofmeister ions [28]. Similarly, Fanaian et al. studied the Hofmeister anions effect on PNIPAM and PNIPAM-*co*-PAA (poly(acrylic acid)) polymer particles, and found that PNIPAM-*co*-PAA microgels exhibited a greater sensitivity to flocculation compared to PNIPAM

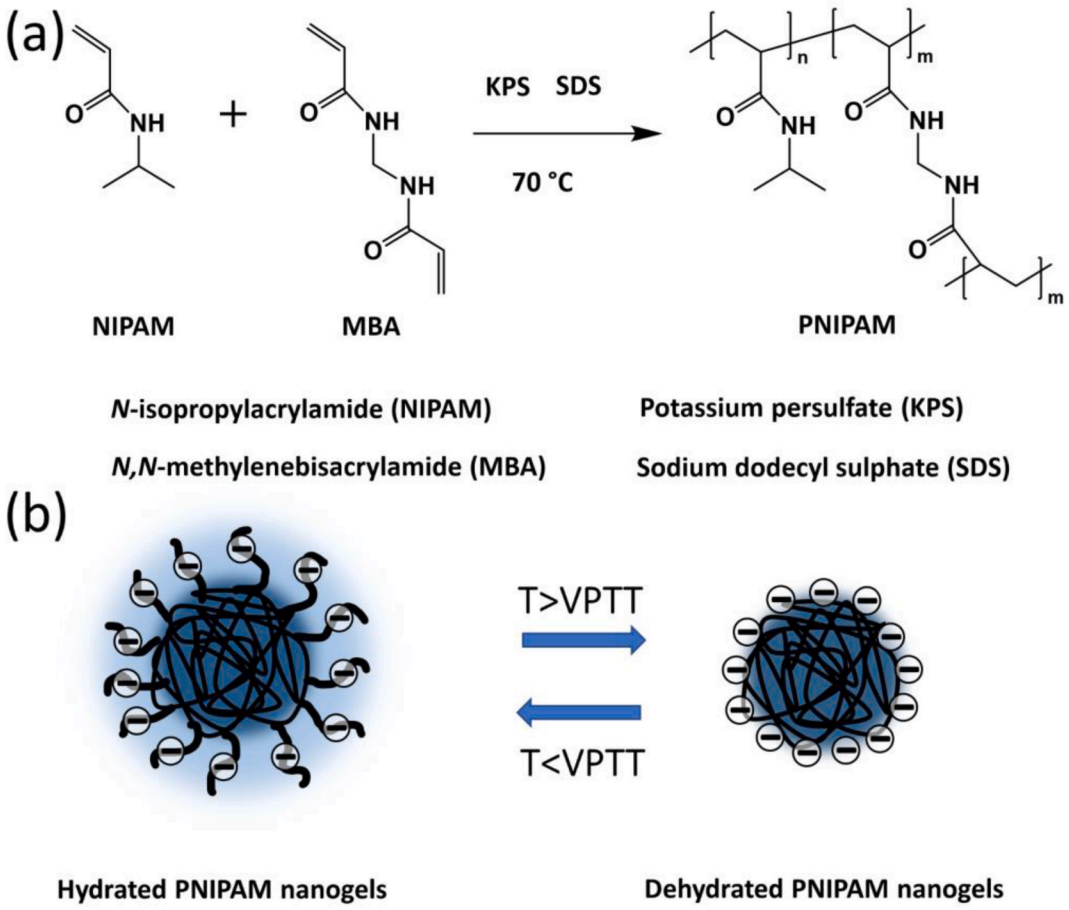

Scheme 1. Schematic representation of PNIPAM synthesis and their thermo-responsive properties. (a) Free radical dispersion polymerization of PNIPAM nanogels and (b) graphical representation of the polymer nanogel response to changes in temperature.

[29]. This increased sensitivity was due to the stronger interaction capacity of those ions with the PAA moieties in the microgels [29]. To use these findings in the practical application of ion identification, Carvalho et al. developed PNIPAM-based optical etalons to investigate how various salts in the Hofmeister series influenced the microgel hydration state by observing the shift of the reflectance peak [30]. Their work revealed the contribution of the counter anion to the swelling behaviour. As such, the understanding of the colloidal stability of the PNIPAM nanogels has improved by employing different experimental approaches. Our work complements and adds new insights to the prior work by comprehensively investigating cation-induced deswelling and flocculating behaviour and morphological changes occurring due to electrolyte interactions. Greater understanding of the combined effect between the cationic valency and temperature on the particle stability holds significant value, in particular for the design of drug delivery systems based on PNIPAM nanogels, where the precise control over flocculation is crucial [18].

In this paper, we investigated the phase and morphological change (i.e., deswelling, aggregation and thermal reversibility behaviour) of PNIPAM nanogels in the presence of multivalent electrolytes (NaCl, KCl, $MgCl_2$, $CaCl_2$ and $AlCl_3$) spanning mono-to tri-valent electrolytes, varying their ionic strength as a function of temperature. Moreover, we implemented a Debye screening model by accounting for the electrostatic interactions, which can be applied to the multivalent electrolyte systems to determine the thickness of the electric double layer. Combination of this model and our experimental work will help further the understanding of the colloidal stability of PNIPAM nanogels in multivalent electrolyte solutions in a predictive way.

2. Results and discussion

2.1. Synthesis of PNIPAM nanogels and their thermo-dependent size variation

Scheme 1 shows the synthesis of the PNIPAM nanogels by free radical dispersion polymerization under an inert environment, forming a 3-dimensional cross-linked polymer particle. These PNIPAM nanogels are sensitive to temperature, *i.e.* they deswell when the temperature increases above their VPTT [5,15]. At this temperature, the PNIPAM nanogels undergo the phase transition from a hydrated state to a dehydrated state, due to the disruption of the amide-water hydrogen bonds [31,32]. Below the VPTT, the hydrophilic polymer chains extend into the continuous phase by forming hydrogen bonds between the polymer and the solvent [33]. On the other hand, when the temperature is above the VPTT, the hydrogen bonding becomes weaker, which results in a contraction of the main chains forming hard globules [33], Scheme 1 (b). Fig. S1 shows a scanning electron microscopy image of dried nanogels and their particle size distribution. In the dried state the particles seem to merge due to their outer shell interactions, yet the electron microscopy images confirm the formation of uniform spherical particles at a diameter range of 170 ± 12 nm.

Following this, we established the colloidal stability behaviour of the PNIPAM nanogels by following the hydrodynamic diameter (D_h) and zeta potential values in aqueous medium as a function of temperature, as shown in Fig. 1 and Fig. S2. The nanogels initially have a D_h of 283 nm with a polydispersity index (PdI) of 0.01 which decreased to 182 nm (PDI = 0.02) with a swelling ratio (a ratio of a swollen D_h (25 °C) to the deswollen D_h (50 °C)) of 1.56, marking a phase transition occurring between 30 °C and 40 °C in Fig. 1 (a). The size change of the nanogels mainly depends on the structural conformation of the polymer chains and the level of hydrogen bonding ability at a given temperature. In this dispersion polymerization, KPS is used as the initiator and the sulphate groups originating from the initiator are therefore located at the polymer chain ends of PNIPAM. This results in the nanogels possessing an anionic surface layer around the cross-linked particle [34]. Given the diffusive properties of the nanogels in swollen state, the measured zeta potential results were slightly smaller in magnitude compared to the hard sphere of same charge density. The surface charge was analysed in zeta potential measurements, which became more negative during the heating process, changing from −7.2 mV at 25 °C to −42.1 mV at 50 °C, Fig. 1 (b). This shift is attributed to the collapse of the swollen PNIPAM nanogels as depicted in Scheme 1 b. Such contraction of the colloidal particle results in an increased surface charge density, *i.e.* the enhanced negative zeta potential. This was also observed by Varga et al. in their exploration of the electrophoretic mobility of PNIPAM particles. While they stated the inner section of the particles behave similarly to a neutral hard sphere, the electrophoretic mobility was induced by the charge in the outer layer of the particles

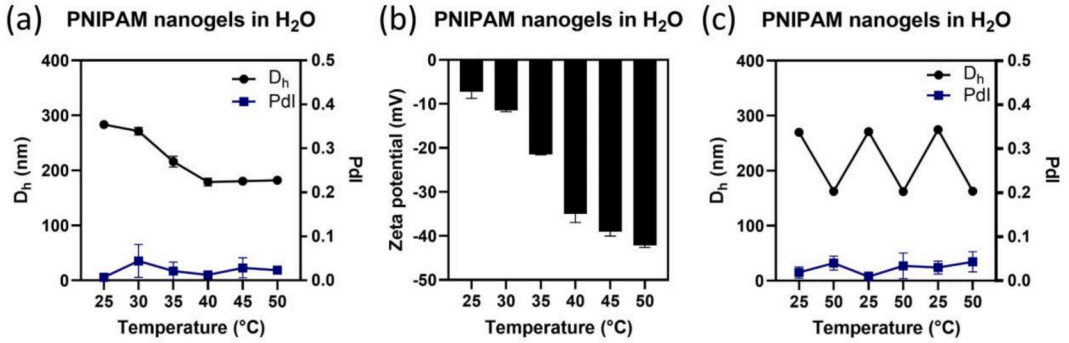

Fig. 1. The thermo-responsive behaviour of the PNIPAM nanogels by dynamic light scattering and zeta potential measurements. (a) Thermal sensitivity of the PNIPAM nanogel hydrodynamic diameter and PdI, (b) zeta potential of the PNIPAM nanogels as a function of temperature, and (c) thermal reversibility shown by diameter changes upon repetitive cycles of heating and cooling (25 °C–50 °C).

[35]. Furthermore, Sierra-Martin et al. reported the effect of increasing the temperature causing the electrophoretic mobility to increase due to the enhanced charge density resulting from particle deswelling. This temperature dependency can offer a means of controlling the electrophoretic mobility, unlike the conventional charged hard spheres where the electrophoretic mobility will likely remain constant during temperature variations [36]. Nevertheless, these synthesised nanogels possess colloidal stability over the whole temperature range tested. Below the VPTT, strong steric stabilization from the solvated dangling chains dominates the stability of nanogels as the lower zeta potential (−7.2 mV) would likely be insufficient to stabilize the nanogels as a dispersion. Above the VPTT where the PNIPAM chains are in the collapsed state, the electrostatic repulsion (−42.1 mV) is responsible for preventing the nanogels from aggregating.

In a cyclic temperature program where the temperature is fluctuated between 25 °C and 50 °C in a consecutive manner, the PNIPAM nanogels demonstrate reversible swelling/deswelling behaviour and their D_h shifts between the 280 nm and 180 nm, repeatedly with no flocculation behaviour, as shown in Fig. 1 (c).

2.2. Colloidal stability of PNIPAM nanogels as a function of ionic strength

In biological media, colloidal particles are exposed to complex ionic interactions that play an important role in their volumetric phase transitions. Therefore, it is important to predict their deswelling, flocculating, and thermal reversibility behaviour under a range of ionic interactions. For this reason, we investigated the effect of the ionic strength on the thermal stability of nanogel dispersions by using mono- and multi-valent cationic electrolytes at different concentrations (0.1 mM–100 mM). The ionic strength of electrolyte solutions containing the different cations can affect their electrical conductivity. As the valency of the electrolytes increased, a non-linear increase in the electrical conductivity with the trend of $Al^{3+} > Ca^{2+} > Mg^{2+} > K^{+} > Na^{+}$ was observed, Fig. S3. Furthermore, the comparative analysis of electrical conductivity between the pure electrolytes and data measured in the presence of PNIPAM nanogels indicate non-specific binding interactions of ions within hydrogels.

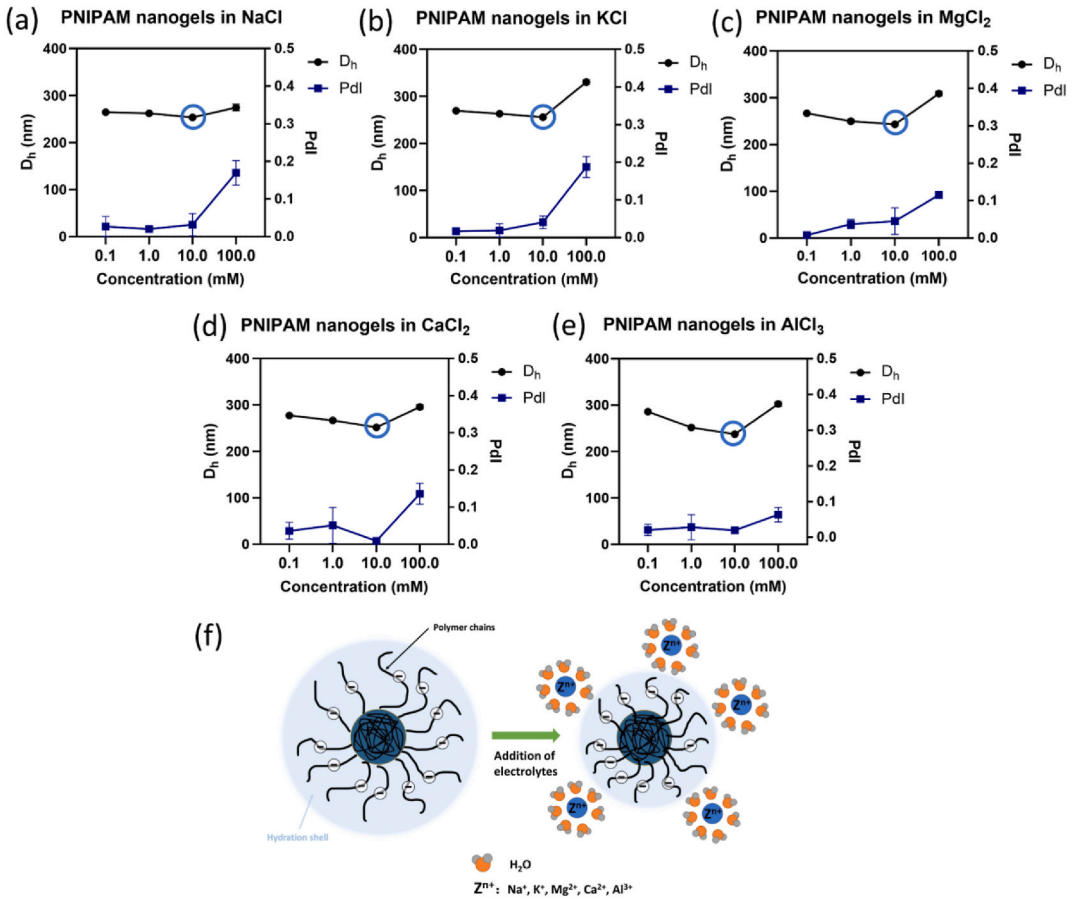

Fig. 2. The deswelling behaviour of PNIPAM nanogels in the multivalent electrolytes over a concentration gradient from 0.1 mM to 100 mM at 25 °C. (a) NaCl, (b) KCl, (c) $MgCl_2$, (d) $CaCl_2$ and (e) $AlCl_3$ and (f) schematic diagram for the hydrated nanogels representing the deswelling mechanism by the added electrolytes. The dark blue circle highlights the minimum diameter that nanogels obtained in the 10 mM electrolyte solution.

2.2.1. Deswelling behaviour of PNIPAM nanogels in multivalent cation solutions

Upon adding electrolytes to the dispersion, the corresponding ionic strength of the suspensions increase and the colloidal stability of nanogels are affected by the ionic interactions [25,37]. The dissociated cations form around the negatively charged PNIPAM nanogels forming an electrical double layer (EDL). The structure and the thickness of the EDL also changes depending on the nature and valency of the cation and contributes to the deswelling power of the PNIPAM as a function of electrolyte type and concentration.

PNIPAM nanogel dispersions had good colloidal stability for all the tested cations (Na^+, K^+, Mg^{2+}, Ca^{2+} and Al^{3+}) below 100 mM ion concentrations at 25 °C (Fig. 2). When the electrolyte concentration reached a 10 mM the deswelling behaviour became more pronounced and the nanogels reached their minimum diameters for all electrolytes (circled in blue in Fig. 2), and all the samples had PdI values ≤ 0.05, indicating that no aggregation had occurred. As the electrolyte concentration increases, water molecules migrate outwards from the hydration shell, causing a decrease in the D_h values obtained from DLS measurements.

In this system, the nanogel hydration sphere consists of a crowded mixture of water molecules, polymer chains, and ions, where each component interacts with the other and hence contributes to the nanogel stability [25]. One of the molecular mechanisms for the deswelling of the PNIPAM nanogels is driven by the cations interacting with the hydration shell of the polymer. At this interface, the water molecules are highly polarized through the hydrogen-bonding of the amide moieties of the polymer pendant groups. Thus, addition of the cations causes dehydration of the hydrophilic amide groups. Alternatively, the osmosis of water from the nanogels in the presence of electrolyte solution may also contribute to the deswelling mechanism [21,38]. It is worth noting that those electrostatic interactions also depend on the diffusion of ions into the 3D network of the nanogel, which is expected to be dependent on the

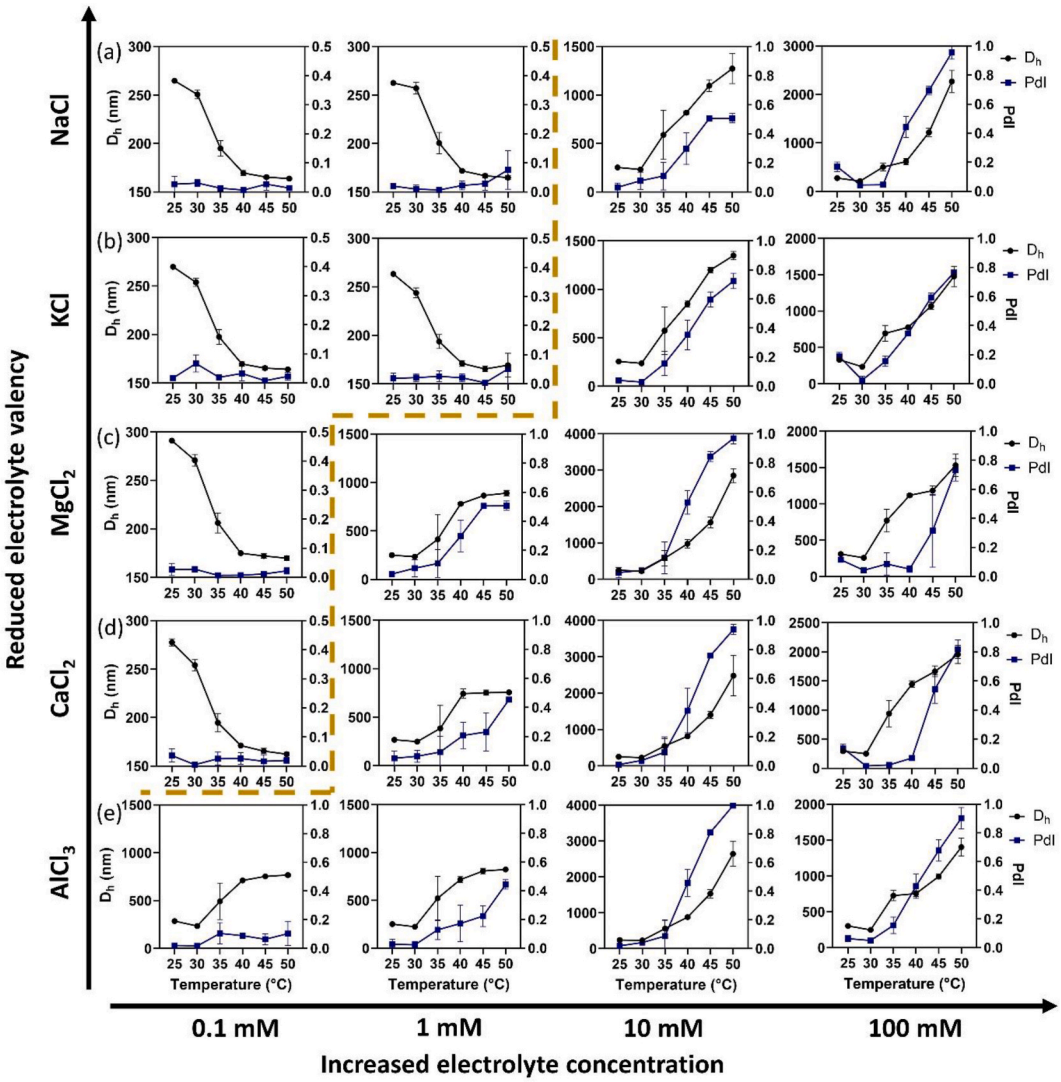

Fig. 3. The flocculation behaviour of PNIPAM nanogels in various electrolytes over the concentration range (0.1 mM–100 mM) and at temperatures between 25 °C and 50 °C. (a) NaCl, (b) KCl, (c) $MgCl_2$, (d) $CaCl_2$ and (e) $AlCl_3$. The dark yellow dash line separates the phase transition from dispersed nanogels to aggregated ones.

cross-linking density of the nanogels. Wu et al. reported that as the cross-linking density is increased, the water diffusion decreases, and the reduction of the diffusion rate is higher at the polymer-water interface [39]. The variation of diffusion coefficient with cross-linking density is related to the variation of water content at different cross-linking densities. The diffusion of ions also decreased as the cross-linking density is increased. We hypothesize this is due to the ability of hydrated cations to induce deswelling of the nanogels by polarizing the water molecules on the polymer chains as sketched in Fig. 2 (f). This effect is more pronounced as valency of the cations increased, *i.e.* the ions with a higher valency have the superior ability to dehydrate the PNIPAM nanogels following the Schulze–Hardy rule [40,41]. Furthermore, for the cations possessing the same valency, the ability to deswell the nanogels is closely related to their charge density. The higher the charge density of the cations, the greater the ability to polarize the water molecules on the polymer chains and hence the higher the shrinkage in the nanogels. Therefore, the deswelling ability was found to be in the order of $Al^{3+} > Mg^{2+} \geq Ca^{2+} > Na^{+} \geq K^{+}$. However, with the further increase in the electrolyte concentration to 100 mM, the stability of the nanogels was decreased and nanogels began to aggregate, as observed with the increase in the D_h and PdI values; D_h of 275 nm (0.17) in Na^{+}, 331 nm (0.19) in K^{+}, 309 nm (0.12) in Mg^{2+}, 296 nm (0.14) in Ca^{2+}, and 302 nm (0.05) in Al^{3+}. This was due to the higher concentration of electrolyte solutions diminishing electrostatic repulsion forces by the screening effect and interaction of cations with the anionic groups on the polymer chains, which thus reduced the stability of nanogels [42,43]. This will be examined in more detail later with the determination of zeta potential values for these nanogels with varying electrolyte concentrations.

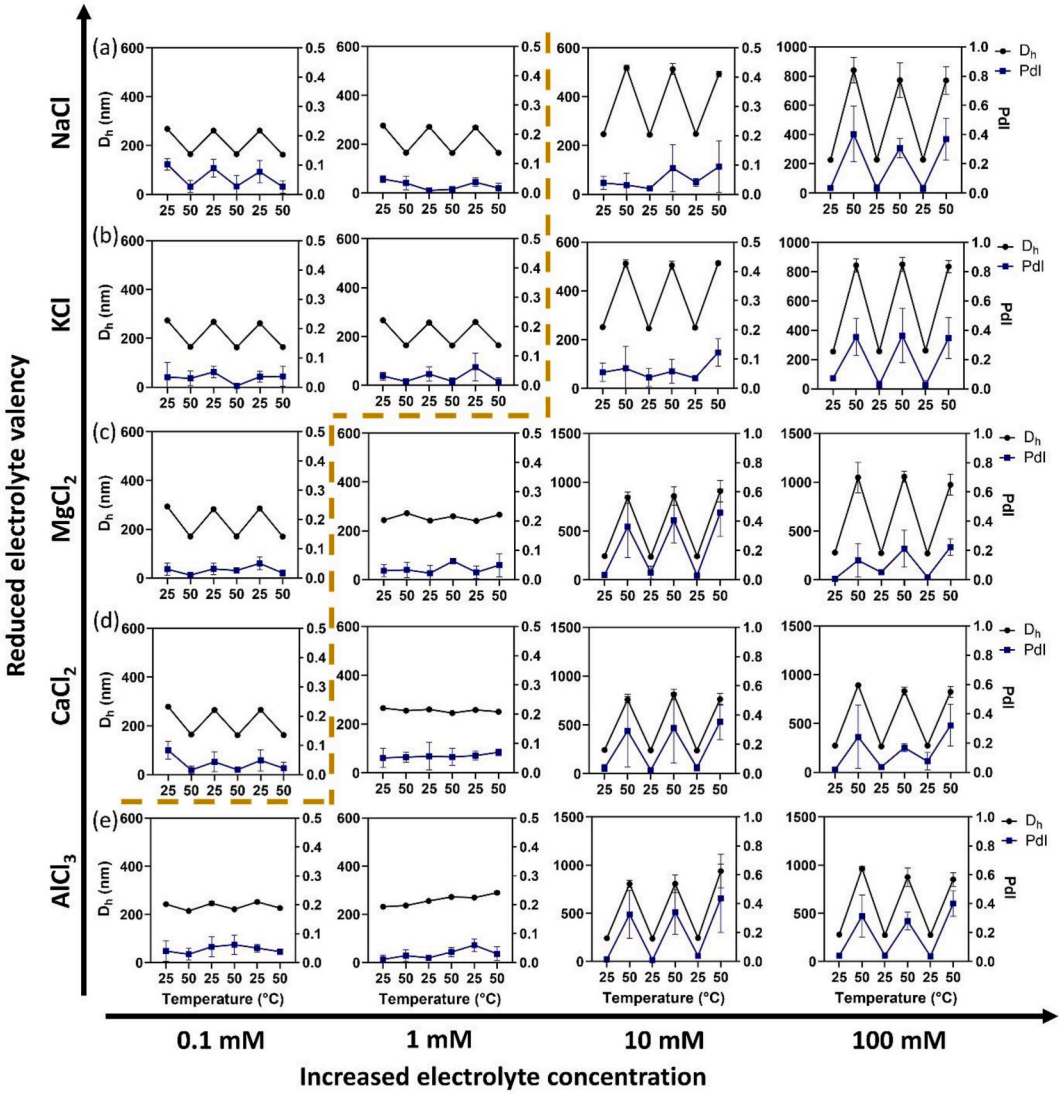

Fig. 4. Thermal reversibility behaviour of aggregated PNIPAM nanogels at their critical flocculation concentration over the repetitive cycles of heating and cooling (25 °C–50 °C). Nanogels in (a) NaCl, (b) KCl, (c) $MgCl_2$, (d) $CaCl_2$, and (e) $AlCl_3$. The dark yellow dash line separates the reversibility fashion of nanogels in the multivalent electrolyte solution.

2.2.2. Flocculation behaviour of PNIPAM nanogels in multivalent cation solutions

We also investigated the flocculation behaviour of PNIPAM nanogels in the presence of those electrolytes without steric repulsion-assisted stabilization by increasing the temperature above the VPTT of the nanogels and quantified the critical flocculation concentration (CFC), *i.e.* the specific concentration that the nanogels in electrolyte solution undergo flocculation at different temperatures.

The resistance of the PNIPAM nanogels to aggregation depended heavily on the stability of their electrical double layer. The addition of electrolyte will affect the net screening effect of charged nanogels by forming a cloud of ions around the nanogels [44]. Both cations and anions in electrolyte system contribute to the ionic strength of a solution, which enables compression of the electrical double layer. Furthermore, chloride ions were reported to demonstrate a significant effect on reducing the VPTT by preventing the water from interacting with amide groups of PNIPAM [23,24,26,37]. However, the cations contribute more to the ionic strength than anions in our studied system according to equation 5. Therefore, the impact of cations was considered as the main driving force on the colloidal stability of PNIPAM nanogels.

Fig. 3 summarizes the flocculation sensitivity of PNIPAM nanogels in a range of multivalent electrolytes at elevated temperatures. As the temperature was raised, nanogels demonstrated the deswelling behaviour below the CFC in their electrolyte solutions, which was observed for both monovalent electrolytes (Na^+ and K^+) below 10 mM and the divalent electrolytes (Mg^{2+} and Ca^{2+}) below 1 mM. The trivalent Al^{3+} on the other hand, flocculated the nanogels at all the concentration ranges tested (even at 0.1 mM). Fig. S4 provided the detailed size information by the multiple angle dynamic light scattering (MA-DLS) on the aggregates formed at the CFC. As a result, we concluded that the CFC of PNIPAM nanogels decreased with the increasing valency of the cations highlighted. We did not observe distinct difference in flocculation behaviour between cations possessing the same valency, which indicated that the power to flocculate nanogels most likely to be similar for within the same range of valency. The heating-induced flocculation behaviour was particularly sensitive to the electrolyte concentration, and it followed the Schulze–Hardy rule, *i.e.* greater the valency of the electrolyte ion, greater will be its coagulation power [40,41].

Due to the impact of cations on the stability of electrical double layer, the valency of cations in electrolyte solutions has an influence on the screening effect: the higher the valency, the stronger the screening effect [45]. However, with the increased ionic strength, the double layer of nanogels will be compressed to a critical point and start to aggregate due to the disrupted screening effect. In general, a divalent ion Mg^{2+} and Ca^{2+} will be more efficient in approaching the aggregation critical point in comparison with a monovalent ion Na^+ and K^+, but demonstrate weaker screening effect than Al^{3+}.

Given all the considerations, we concluded the combined stability was mainly driven through the ionic strength and temperature of the PNIPAM nanogels in the electrolyte solution and these two effects can counteract each other in certain scenarios. The increased ionic strength diminishes the electrostatic repulsion force by the screening effect, and the elevated temperature decreases steric stabilization due to the phase transition, which together promote the formation of aggregates [5,15,46,47].

2.2.3. Thermal reversibility behaviour of PNIPAM nanogels in multivalent cation solutions

Further to understanding particle phase and morphology, we also accounted for size reversibility of PNIPAM nanogels in electrolyte solutions over the tested concentration range under cyclic heating and cooling treatment. As illustrated above that nanogels demonstrated the deswelling/swelling reversibility below the critical flocculation concentration upon the heating and cooling treatment, we also studied the flocculation power of multivalent electrolytes on the PNIPAM which follows the Schulze-Hardy's rule but have not tested the reversibility of this process. Here, we investigate another mode of thermal reversibility, where the flocculated nanogels return to dispersed state while cooling down below VPTT, i.e., aggregation/dispersion reversibility.

Fig. 4 shows that nanogels exhibited thermal reversibility in deswelling/swelling and aggregation/dispersion behaviour in multivalent electrolyte solutions and these different size reversibility trends were separated by the yellow dash line. For the thermally triggered swelling/deswelling ability, nanogels were free to demonstrate their phase reversibility in the low electrolyte concentrations in which the electric repulsion is strong enough to stabilize the nanogels to avoid aggregations. One should bear in mind that above the VPTT, this stability is purely electrostatic and not due to steric repulsion. Nevertheless, these aggregated nanogels can redisperse with cooling treatment. This is due to the weak aggregation of nanogels, and they regain steric repulsion by extending their polymer chains in the medium below the VPTT.

2.2.4. Morphological analysis of PNIPAM nanogels in multivalent cation solutions

We further analysed the dynamic flocculation behaviour of the nanogels using an in-situ imaging analysis under polarised optical microscopy by observing the particle aggregation at the sessile droplet edge during heating cycles. To capture the PNIPAM nanogels in the optical microscopy set-up, the suspensions were stained by methylene blue. The aggregation of the particles was recorded in multivalent salt solutions whilst applying fast heating and cooling cycles using a VAHEAT® stage. Fig. S5 are a series of snapshot images from the supporting videos recorded at the sessile droplet edge depicting spontaneous aggregation of the particles as the concentration of the cations increased. The videos further provide additional evidence that the multivalent electrolytes demonstrate greater flocculation power on nanogels than monovalent ones, i.e. $Al^{3+} > Mg^{2+} = Ca^{2+} > Na^+ = K^+$, and the response rate to form aggregates was consistent to the order of the flocculation power. Such in-situ analysis particularly suggested that the phase transition behaviour of those nanogels from the dispersion to the aggregation strongly depends on the cationic valency of electrolytes they are dispersed in, which is consistent to the Schulze–Hardy rule.

Previous works claimed the tendency of the polymer chains to retract during heat cycles which can cause local density differences within the particle's inner core and outer shells [17,18,48]. Following upon this, we hypothesized that the presence of the ions could influence the contraction of the polymer branches at the polymer-ion interface, resulting in the denser and stiffer outer layer of polymer particles. To assess this hypothesis, we analysed the higher resolution morphology and the stiffness of the nanogels using TEM

and AFM. The images in Fig. 5 of the nanogel particles represents the formation of a smooth surface on the nanogels dried from an aqueous medium. In contrast to this, the nanogels dried in the presence of electrolyte solutions, demonstrated higher contrast and roughness in the outer shell. Such change in their outer surface morphology indicates a stiffer polymer interface. This morphological difference between the bulk of the nanogels and the ones with a 5–10 nm shell can be attributed to accumulation of the ions within the polymer chains which can cause ionically linked hard shells. The presence of this hard-shell effect becomes more significant as the cation valency is increased. Therefore, the TEM images and AFM stiffness mapping plots confirms that in the dry state the particle morphology varies between the outer shells and the core structure. Although there is a likely morphological change due to drying, to avoid these effects, the relative concentration of the ions was kept constant at 1 mM to present a comparable result and the samples were rinsed on the TEM substrate. Further investigation using a liquid cell in TEM or AFM may be considered to confirm the correlation of this effect in wet state.

2.3. Zeta potential and Debye screening effect in electrolyte solution

We followed the changes in the electrostatic potential of the colloids by measuring the zeta potential of the PNIPAM nanogels in different electrolyte solution at 25 °C and 50 °C which is summarized in Fig. 6 (a) and (b), respectively. As the ionic strength determined by the electrolyte concentration and their cationic valency is increased, it is expected that the zeta potential of the nanogel dispersion becomes less negative. Increasing the temperature also triggers a deswelling or flocculation behaviour and drives the zeta potential of nanogels shifts to more negative values for each concentration point against an individual electrolyte system. This is attributed to the screening effect demonstrated by the multivalent electrolytes and the heating-induced enhancement of nanogels charge density [15]. At a 10 mM concentration however, we observed an intriguing reversal of the zeta potential in $AlCl_3$ system shifting to a positive value at 25 °C in Fig. 6 (a) and (b). Such flip in the zeta potential was also seen in nanoparticles since higher valency of cations can easily cross the electrical double layer and bind to surface of sample [49,50].

Furthermore, with the temperature increase to 50 °C, the overall zeta potential for mono- and divalent ions shift to more negative values at higher electrolyte concentration while trivalent electrolytes showed more positive in the zeta potential, Fig. 6 (b). Such enhanced zeta potential can be explained by the heating-induced enhancement of charge density on nanogels. The ability of cations to neutralize the charged nanogels, *i.e.* Debye screening effect, follows the trend ($Al^{3+} > Mg^{2+} > Ca^{2+} > Na^{+} > K^{+}$). As the electrolyte concentration increases from 0.1 mM to 100 mM at the constant temperature, *e.g.* 25 °C, the zeta potential of nanogels becomes less negative in their electrolyte system and the higher valency of electrolyte is able to screen more surface charge of nanogels than monovalent electrolyte. This is because the ionic strength of electrolyte solution determines the Debye length of the screening cloud on the colloidal sample [51]. When the nanogels were in a concentrated electrolyte or higher cationic valency of electrolyte solution, effective zeta potential will be reduced in magnitude, as it is shielded by the presence of the counter-ions in the Debye-Hückel screening cloud.

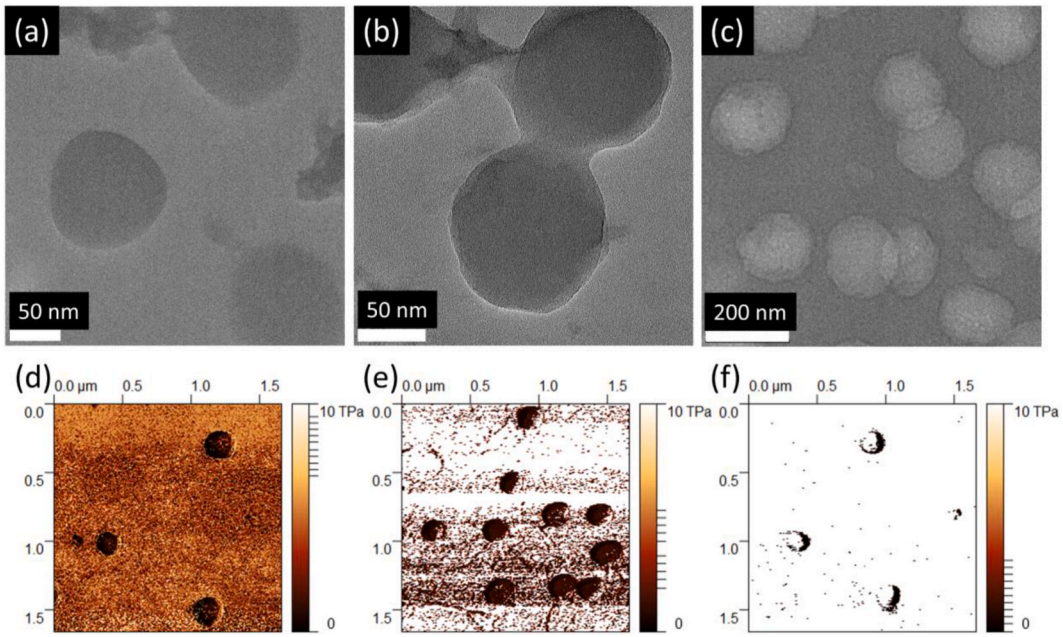

Fig. 5. Bright field (BF) TEM images and AFM stiffness maps demonstrating the morphology and the mechanical contrast in the PNIPAM nanogels dried from various electrolyte solutions (a and d) TEM image and the AFM stiffness map of the particles dried from aqueous medium (no-shell), (b and e) TEM image and the AFM stiffness map of the particles dried from 1 mM NaCl solution presenting a softer-shell and (c and f) TEM image and the AFM stiffness map of the particles dried from 1 mM $AlCl_3$ solution presenting a harder-shell.

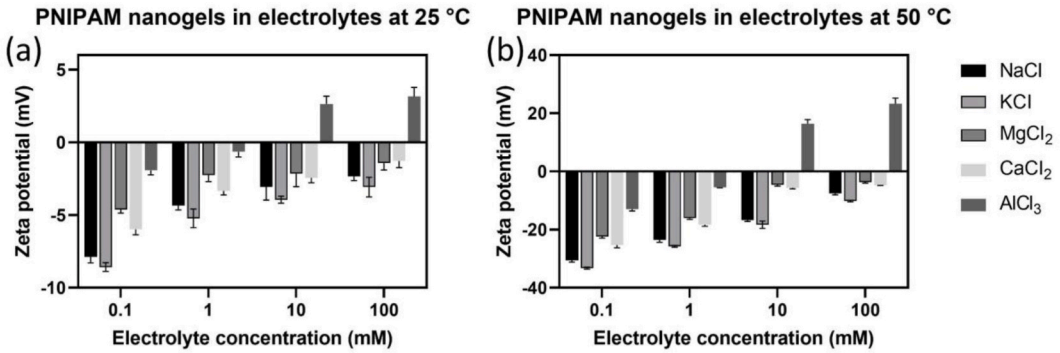

Fig. 6. Zeta potential of PNIPAM nanogels in various electrolyte solution at a gradient concentration range over the temperature between the 25 °C and 50 °C.

To explain the effect of electrostatic interactions on the zeta potential in a predictive way, we followed the Debye screening model, equation (3) and simulated the Debye length using the Wolfram Mathematica 13.1®. In this model, the theoretical Debye length and electrical potential was acquired as a function of distance, valency, and concentration based on equations (3) and (4). The influence of electrolyte concentration on the Debye length is significant. Therefore, to ensure the comparability of our results, the electrolyte concentrations were standardised to 0.1 M. At this concentration, the Debye lengths for mono-, di-, and trivalent cations are ~1 nm, 0.56 nm, and 0.39 nm, respectively. In addition, the particle charge (q) parameter was obtained by fitting the DLVO equation with experimental data of monovalent particles in Wolfram Mathematica 13.1®. The acquired data presented in Fig. S6 shows the expected decrease of the Debye length as a function of increased cationic valency. Such behaviour is expected from the model, indicating that the magnitudes of the compression of the electrical double layer shown in the model accurately matched the trend for the dropping zeta potential of nanogels in the different electrolyte systems, with the Al^{3+} ions showing the most significant potential for electrostatic screening. It is important to note that our model assumes a hard sphere for the nanogels that does not fully represent the morphology of the nanogels in the swollen state. In the swollen state nanogels are known to possess a diffusely crosslinked architecture in which the crosslinking density may differ between the core and the shell [52]. This discrepancy between the model and experimental reality may explain the differences between the model and the experimental data. For example, the zeta potential of the nanogels demonstrates a reversal of surface charge in Fig. 6, when the concentration of Al^{3+} ions reach 10 mM. The Debye screening model used in this work did not predict such reverse in surface charges. This inconsistency between the model and the experimental results can be attributed to the effect of multiple coordination of the nanogel end groups due to the presence of the surfactant-SDS with the Al^{3+} ions which could potentially shift the electric double layer formation. Furthermore, the strong ionic compression induced by Al^{3+} cations, possess a dimensional mismatch between the theoretical Debye length (~0.39 nm) compared to the size of the hydrated radius of Al^{3+} ions (~0.45 nm) [53,54]. Therefore, the zeta potential reversal presents an indication of disruption of the electrical double layer in the presence of the Al^{3+}.

3. Conclusions

In this study, we studied the interplay between colloidal stability, thermal reversibility, agglomeration, and morphological transition of PNIPAM nanogels in multivalent electrolyte solutions over the tested temperatures between 25 °C and 50 °C.

Our work revealed that the presence of the electrolytes caused the PNIPAM nanogels to reduce in size reaching their minima at 10 mM. The deswelling ability and destabilization effect of the cations was found to be in the order of $Al^{3+} > Mg^{2+} \geq Ca^{2+} > Na^{+} \geq K^{+}$. Similarly, the critical flocculation concentration was 10 mM for the monovalent cations, 1 mM for divalent cations and 0.1 mM for trivalent cations, which is predicted by the Schulze–Hardy rule. The morphology and stiffness of dried colloidal particles was analysed by TEM and AFM. The dried nanogels presented the formation of a shell-like layer surrounding the particles which may be driven by electrolyte driven polymer chain stiffening on the particle surface. The TEM further revealed this shell to vary in density as a result of the electrolyte interactions, i.e. the soft-shell structure became harder/stiffer in multi-valent electrolytes. Additionally, we observed a thermally induced size reversibility in the aggregated nanogels and confirming weak interactions within the nanogel clusters.

A Debye length model was used to predict the electrolyte-induced screening process. According to our experimental and modelling data, at the concentrations of 10 mM and 100 mM, trivalent cation (Al^{3+}) seems to disrupt the electrical double layer. Whereas the experimental and modelling data indicated that the Al^{3+} at 0.1 mM and 1 mM as well as the divalent cations (Ca^{2+} and Mg^{2+}) compressed the electric double layer substantially compared to the monovalent cations (Na^{+} and K^{+}). Overall, our work clearly validated the earlier studies on the electrostatic and interfacial properties of PNIPAM nanogels and provided further evidence on the parameter space on their stability whilst accounting for the morphological changes in these electrolytes. Further work involving the effect of the counter anions and wet state morphological changes would be beneficial to further our understanding of these colloidal systems. The insights provided by our work will assist in the design of responsive nanogels by allowing the tuning of the colloidal stability and swelling transitions according to the required applications by utilising multivalent ions.

4. Experimental section

4.1. Materials

Sodium chloride (NaCl, ≥99 %), potassium chloride (KCl, ≥99 %), magnesium chloride ($MgCl_2$, ≥95 %), calcium chloride dihydrate ($CaCl_2 \bullet 2H_2O$, ≥99 %), methylene blue hydrate (MB, ≥95 %), *N*-isopropylacrylamide (NIPAM, 97 %), *N,N*-methylenebisacrylamide (MBA, 99 %), potassium persulfate (KPS, ≥99 %), and sodium dodecyl sulphate (SDS, ≥99 %) were purchased from Sigma-Aldrich Company Co., Ltd. (UK). Aluminium chloride ($AlCl_3$, 99 %) was purchased from Thermo Fisher Scientific (UK). Deionized water (18 MΩ cm^{-1} resistivity) was supplied from a molecular water purification system, Purite Fusion 160 (SUEZ).

4.2. Synthesis of PNIPAM nanogels

The PNIPAM nanogels were synthesised by free radical dispersion polymerization as detailed in Scheme 1 [17]. In short, a mixture of NIPAM monomer (131.2 mM), MBA cross-linker (9.7 mM), and SDS surfactant (0.6 mM) were dissolved in deionized water (117.5 mL) in a 250 mL two-neck round bottom flask. This system was attached to a reflux condenser and a magnetic stirrer and then sealed with a rubber septum. The dissolved oxygen was degassed by bubbling the solution with nitrogen for 1 h under stirring at 400 rpm. Separately, KPS initiator (2.2 mM in 7.5 mL deionized water) solution was degassed with nitrogen for 1 h. The round bottom flask was then heated to 70 °C and the initiator was injected by a syringe into the heated solution. The reaction was allowed to continue for 4 h at 70 °C under a nitrogen atmosphere. To terminate the reaction, the round bottom flask was opened to air and placed in an ice-bath for 30 min. To purify the PNIPAM nanogels, the reaction mixture was transferred to dialysis tubes (12–14 kDa MWCO, Spectrum Labs) and dialyzed for 5 days, changing the water twice daily. The purified suspension was then lyophilized (Virtis Benchtop K with ultra-low temperature condenser) and stored in a desiccator.

4.3. Preparation of PNIPAM nanogel dispersions in various electrolyte solutions

The electrolyte solutions (NaCl, KCl, $MgCl_2$, $CaCl_2$ and $AlCl_3$) were prepared at the concentrations of 0.1 mM, 1 mM, 10 mM, and 100 mM [cation] with deionized water. The concentration of PNIPAM nanogels in the respective electrolyte solution was kept at 0.01 wt%. This suspension was fully dispersed using a sonication bath (Clifton SW3H, work at 280 W power) for 3 h before performing the size distribution and zeta potential measurement as a function of temperature. The temperature of the bath was kept below 25 °C during the period of sonication.

4.4. Particle size distribution

The particles sizes, *i.e.* hydrodynamic diameter (D_h), were measured using a Malvern Zetasizer Ultra (laser wavelength of 633 nm (He–Ne), scattering angle 173°, medium viscosity 0.8872 mPa s, medium refractive index 1.330) DLS system. Since aggregated particles on micro scale irradiated by the laser light gives an inhomogeneous scatter pattern, it is necessary to accurately measure their scattering profile from the multiple detection angle. To achieve higher resolution particle size distribution of agglomerated nanogels at the elevated temperature (50 °C), multi-angle dynamic light scattering (MA-DLS) was exploited to acquire the combined scattering information, and the intensity of light scattered by agglomerated particles was collected at the back scatter 173°, side scatter 90°, and forward scatter 45°, respectively. Before the measurements, all samples were treated with the ultra-sonication bath for 0.5 h to ensure the colloidal particles were freely suspended. The Z-average diameter was recorded in the range between 25 °C and 50 °C at the interval of 5 °C using a thermal equilibration time of 300 s at each temperature change in a folded capillary cell (DTS1070, Malvern). After the measurement was performed at 50 °C, the thermal reversibility of PNIPAM nanogels was tested by applying a cooling treatment to 25 °C with the same thermal equilibration time (300 s). For the measurement in a cyclic temperature program, the temperature oscillates between 25 °C and 50 °C in a consecutive manner with the same thermal equilibration time (300 s) at each oscillation. Capillary cells were flushed with ethanol and water prior to usage. Measurements were repeated in triplicate to give a mean Z-average diameter and polydispersity index (PdI).

To verify the DLS measurements electron microscopy imaging was performed. For this reason, a TESCAN MIRA II, field-emission high-resolution analytical scanning electron microscopy (SEM) was used. Prior to imaging, the dispersion of PNIPAM nanogels (0.001 wt%) in an aqueous medium were cast directly onto the flat aluminium stubs and dried at room temperature for the size distribution analysis. Furthermore, the nanogels dispersed in the electrolyte solutions over a range of concentrations were prepared onto a square silicon wafer (5 by 5 mm) using the same preparation method for the morphological observation of aggregates. Following this, the samples were coated by a Quorum Q150T sputter coater with an Au/Pd target. A coating current of 40 mA and coating time of 10 s was used to attain 6 nm thickness to eliminate the charging on the samples caused by electron accumulation. The imaging was done at a 5 kV accelerating voltage with the signal from secondary electrons using an in-lens detector. The electron microscopy image was analysed using ImageJ for the size determination of fully dispersed PNIPAM nanogels. A histogram of size distribution was created by randomly selecting 300 particles from the image and then fitted with a Gaussian function:

$$f(x) = \frac{1}{\sigma\sqrt{2\pi}} e^{-\frac{1}{2}\left(\frac{x-\mu}{\sigma}\right)} \quad (1)$$

where x is the size of the particle, μ is the mean size, and σ is standard deviation of the particle size.

4.5. Dynamics of the phase change and aggregation of PNIPAM nanogels

The temperature-dependent agglomeration of the PNIPAM particles were monitored and recorded in real-time with precise and dynamic temperature control using a custom-made optical microscopy (Olympus, BX53 M) set-up equipped with VAHEAT- Micro heating system (Interherence GmbH). The aliquots of 50 μl premixed PNIPAM particles in electrolytes were mixed with 10 μl methylene blue solutions (0.1 mM) uniformly to induce contrast in imaging of the particles and the homogeneous suspensions were applied onto the smart substrate (poly(dimethysiloxane) reservoirs, SmS–R - 16). The agglomeration of the particles was recorded under a heating program where the temperature is manipulated through a proportional-integral-derivative controller to the define temperature (50 °C). The response time for PNIPAM nanogels to form aggregates was recorded to evaluate the flocculation ability of different electrolyte solutions to nanogels.

4.6. Particle morphology analysis

To analyse the shell softness of nanogels dried from different dispersants, the transmission electron microscopy (TEM) analysis was performed using a 200 kV Talos TEM (FEI Talos F200X) in bright field mode, the images were collected using the Velox software. Prior to imaging, a droplet of nanogels (5 μl, 0.01 wt%) in the electrolyte solutions including aqueous medium, 1 mM NaCl, and 1 mM $AlCl_3$ solutions were cast on the holey-carbon TEM grids with 400-mesh copper for TEM imaging and dried at room temperature. Additionally, atomic force microscopy (AFM, Bruker Multimode 8) was employed to assess the stiffness of nanogels in Peak Force quantitative nanomechanical mapping (QNM) mode with RTESPA-150 probe (tip radius: 8 nm, spring constant: 5 N/m, frequency: 150 kHz). Prior to imaging, a droplet of nanogels (5 μl, 0.01 wt%) in the electrolyte solutions including aqueous medium, 1 mM NaCl, and 1 mM $AlCl_3$ solutions were cast on a silicon wafer (5 × 5 mm) for AFM imaging. The droplets were allowed to dry in ambient conditions overnight.

4.7. Stability of colloidal suspension

The Malvern Zetasizer Ultra DLS instrument was used to carry out aqueous electrophoretic mobility measurements for the nanogels dispersed in the electrolyte solution. Zeta potential is related to the electrophoretic mobility by the Henry function as shown in equation (2) [55]. Therefore, calculation of zeta potential from the mobility is straightforward for systems that fit the Smoluchowski model [56]. Zeta potential measurements were performed in a sampling cuvette (DTS1070, Malvern) at a voltage of 150 V with a minimum of 10 and maximum of 40 runs. This measurement was repeated in triplicate and the average results were presented with a standard deviation.

$$U_E = \frac{2\varepsilon z f(\kappa a)}{3\eta} \tag{2}$$

where U_E is the electrophoretic mobility, z is the zeta potential, ε is the dielectric constant, η is the viscosity, and f(κa) is the Henry's function.

4.8. Debye length in electrolyte solution

The Debye screening model was built up to predict the relationship between the electrostatic field around the charged particles and the ionic strength of the solution [57]. In this model, a charged object in an electrolyte solution experiences a screening effect due to the electrolyte ions clustering near the charged object. This model was simulated by the Wolfram Mathematica program based on equations (3) and (4), which calculates the theoretical electrical potential against the distance from the surface of charged nanogel particles. Furthermore, it can be adapted to investigate the Debye length and electrical potential in the presence of multivalent electrolytes (NaCl, KCl, $MgCl_2$, $CaCl_2$ and $AlCl_3$) over a gradient concentration.

Debye length is the thickness of the electrical double layer and defined as below:

$$\kappa^{-1} = \sqrt{\frac{\varepsilon_r \varepsilon_o \kappa_B T}{2e^2 I}} \tag{3}$$

where I is the ionic strength of the electrolyte , ε_o is the vacuum permittivity, ε_r is the dielectric constant, κ_B is the Boltzmann constant, T is the absolute temperature in Kelvin and e is the elementary charge.

The electric potential of a charged particle (q) against the distance (r) is expressed as

$$V(r) = \frac{q}{4\pi\varepsilon_r\varepsilon_o r} e^{-\frac{r}{\kappa^{-1}}} \tag{4}$$

where ε_o is the vacuum permittivity, ε_r is the dielectric constant, e is the Euler constant and κ^{-1} is the Debye length.

CRediT authorship contribution statement

Yuchen Zhu: Writing – review & editing, Writing – original draft, Methodology, Formal analysis, Data curation, Conceptualization. **Jiaxin Hou:** Writing – review & editing, Validation, Formal analysis. **Dominic M. Gray:** Writing – original draft, Methodology, Data curation. **Tom O. McDonald:** Writing – review & editing, Writing – original draft, Supervision. **Ahu Gümrah Dumanli:** Writing – review & editing, Writing – original draft, Validation, Supervision, Resources, Project administration, Methodology, Funding acquisition, Conceptualization.

Declaration of competing interest

The authors declare the following financial interests/personal relationships which may be considered as potential competing interests:Ahu Gumrah DUMANLI reports financial support was provided by bp-ICAM. Yuchen ZHU reports financial support was provided by China Scholarship Council (CSC).

Acknowledgements

The authors would also like to acknowledge the funding from CSC scholarship for stipend funding (YZ), bp for the bp-ICAM Kathleen Lonsdale Research Fellowship (AGD), Royal Society for the Royal Society Research Grant RGS\R2\202434 (AGD) and EPSRC for funding (EP/S012265/1) (DG and TM). This work was also supported by the Henry Royce Institute for Advanced Materials, funded through EPSRC grants EP/R00661X/1, EP/S019367/1, EP/P025021/1 and EP/P025498/1.

Appendix A. Supplementary data

Supplementary data to this article can be found online at https://doi.org/10.1016/j.heliyon.2024.e32184.

References

[1] J. Brijitta, B.V.R. Tata, T. Kaliyappan, Phase behavior of poly(N-isopropylacrylamide) nanogel dispersions: temperature dependent particle size and interactions, J. Nanosci. Nanotechnol. 9 (2009) 5323–5328.
[2] B.V.R. Tata, J. Brijitta, R.G. Joshi, Thermo-responsive nanogel dispersions: dynamics and phase behaviour, Int J Adv Eng Sci Appl Math 5 (2013) 240–249.
[3] M.J. Ansari, R.R. Rajendran, S. Mohanto, U. Agarwal, K. Panda, K. Dhotre, R. Manne, A. Deepak, A. Zafar, M. Yasir, S. Pramanik, Poly(N-isopropylacrylamide)-Based hydrogels for biomedical applications: a review of the state-of-the-art, Gels 8 (2022).
[4] J.S. Scarpa, D.D. Mueller, I.M. Klotz, Slow Hydrogen-Deuterium Exchange in a Non-α-helical Polyamide, vol. 2, 1967, pp. 6024–6030.
[5] A.R. Town, J. Taylor, K. Dawson, E. Niezabitowska, N.M. Elbaz, A. Corker, E. Garcia-Tuñón, T.O. McDonald, Tuning HIV drug release from a nanogel-based in situ forming implant by changing nanogel size, J. Mater. Chem. B 7 (2019) 373–383.
[6] L. Zha, B. Banik, F. Alexis, Stimulus responsive nanogels for drug delivery, Soft Matter 7 (2011) 5908–5916.
[7] H. Zhang, Y. Zhai, J. Wang, G. Zhai, New progress and prospects: the application of nanogel in drug delivery, Mater. Sci. Eng. C 60 (2016) 560–568.
[8] A. Halperin, M. Kröger, F.M. Winnik, Poly(N-isopropylacrylamide) phase diagrams: fifty years of Research, Angewandte Chemie - International Edition 54 (2015) 15342–15367.
[9] M. Handa, A. Singh, S.J.S. Flora, R. Shukla, Stimuli-responsive polymeric nanosystems for therapeutic applications, Curr Pharm Des 28 (2021) 910–921.
[10] J. Zhang, S. Yun, Y. Du, A.C.W. Zannettino, H. Zhang, Fabrication of a cartilage patch by fusing hydrogel-derived cell aggregates onto electrospun film, Tissue Eng Part A 26 (2020) 863–871.
[11] C.T. Schwall, I.A. Banerjee, Micro- and nanoscale hydrogel systems for drug delivery and tissue engineering, Materials 2 (2009) 577–612.
[12] S. Ashraf, H.K. Park, H. Park, S.H. Lee, Snapshot of phase transition in thermoresponsive hydrogel PNIPAM: role in drug delivery and tissue engineering, Macromol. Res. 24 (2016) 297–304.
[13] R. Dong, B. Guo, Smart wound dressings for wound healing, Nano Today 41 (2021) 101290.
[14] B. Li, D. Li, Y. Yang, L. Zhang, K. Xu, J. Wang, Study of thermal-sensitive alginate-Ca2+/poly(N-isopropylacrylamide) hydrogels supported by cotton fabric for wound dressing applications, Textil. Res. J. 89 (2019) 801–813.
[15] A. Town, E. Niezabitowska, J. Kavanagh, M. Barrow, V.R. Kearns, E. García-Tuñón, T.O. McDonald, Understanding the phase and morphological behavior of dispersions of synergistic dual-stimuli-responsive poly(N-isopropylacrylamide) nanogels, J. Phys. Chem. B 123 (2019) 6303–6313.
[16] L. Johnson, D.M. Gray, E. Niezabitowska, T.O. McDonald, Multi-stimuli-responsive aggregation of nanoparticles driven by the manipulation of colloidal stability, Nanoscale 13 (2021) 7879–7896.
[17] A. Town, E. Niezabitowska, J. Kavanagh, M. Barrow, V.R. Kearns, E. García-Tuñón, T.O. McDonald, Understanding the phase and morphological behavior of dispersions of synergistic dual-stimuli-responsive poly(N-isopropylacrylamide) nanogels, J. Phys. Chem. B 123 (2019) 6303–6313.
[18] L. Johnson, D.M. Gray, E. Niezabitowska, T.O. McDonald, Multi-stimuli-responsive aggregation of nanoparticles driven by the manipulation of colloidal stability, Nanoscale 13 (2021) 7879–7896.
[19] M. Rasmusson, A. Routh, B. Vincent, Flocculation of microgel particles with sodium chloride and sodium polystyrene sulfonate as a function of temperature, Langmuir 20 (2004) 3536–3542.
[20] C.M. Burba, S.M. Carter, K.J. Meyer, C.v. Rice, Salt effects on poly(N-isopropylacrylamide) phase transition thermodynamics from NMR spectroscopy, J. Phys. Chem. B 112 (2008) 10399–10404.
[21] M.S. Khan, G.T. Khan, A. Khan, S. Sultana, Preparation and characterization of novel temperature and pH sensitive (NIPAM-co-MAA) polymer microgels and their volume phase change with various salts, Polymer (Korea) 37 (2013) 794–801.
[22] K.J. Pastoor, C.V. Rice, Cation effects on the phase transition of N-isopropylacrylamide hydrogels, Macromol. Chem. Phys. 216 (2015) 1024–1032.
[23] T.J. Murdoch, J.D. Willott, W.M. De Vos, A. Nelson, S.W. Prescott, E.J. Wanless, G.B. Webber, Influence of anion hydrophilicity on the conformation of a hydrophobic weak polyelectrolyte brush, Macromolecules 49 (2016) 9605–9617.
[24] T.J. Murdoch, B.A. Humphreys, J.D. Willott, K.P. Gregory, S.W. Prescott, A. Nelson, E.J. Wanless, G.B. Webber, Specific anion effects on the internal structure of a poly(N-isopropylacrylamide) brush, Macromolecules 49 (2016) 6050–6060.

[25] E. Daly, B.R. Saunders, A study of the effect of electrolyte on the swelling and stability of poly(N-isopropylacrylamide) microgel dispersions, Langmuir 16 (2000) 5546–5552.
[26] K.J. Pastoor, C.V. Rice, Anion effects on the phase transition of N-isopropylacrylamide hydrogels, J. Polym. Sci. Polym. Chem. 50 (2012) 1374–1382.
[27] E. Daly, B.R. Saunders, Temperature-dependent electrophoretic mobility and hydrodynamic radius measurements of poly(N-isopropylacrylamide) microgel particles: structural insights, Phys. Chem. Chem. Phys. 2 (2000) 3187–3193.
[28] T. López-León, A. Elaïssari, J.L. Ortega-Vinuesa, D. Bastos-González, Hofmeister effects on poly(NIPAM) microgel particles: macroscopic evidence of ion adsorption and changes in water structure, ChemPhysChem 8 (2007) 148–156.
[29] S. Fanaian, N. Al-Manasir, K. Zhu, A.L. Kjøniksen, B. Nyström, Effects of Hofmeister anions on the flocculation behavior of temperature-responsive poly(N-isopropylacrylamide) microgels, Colloid Polym. Sci. 290 (2012) 1609–1616.
[30] W.S.P. Carvalho, C. Lee, Y. Zhang, A. Czarnecki, M.J. Serpe, Probing the response of poly (N-isopropylacrylamide) microgels to solutions of various salts using etalons, J. Colloid Interface Sci. 585 (2021) 195–204.
[31] O. Ramon, E. Kesselman, R. Berkovici, Y. Cohen, Y. Paz, Attenuated total reflectance/fourier transform infrared studies on the phase-separation process of aqueous solutions of poly(N-isopropylacrylamide), J. Polym. Sci. B Polym. Phys. 39 (2001).
[32] H. Lai, P. Wu, A infrared spectroscopic study on the mechanism of temperature-induced phase transition of concentrated aqueous solutions of poly(N-isopropylacrylamide) and N-isopropylpropionamide, Polymer (Guildf) 51 (2010) 1404–1412.
[33] T.Y. Wu, A.B. Zrimsek, S.v. Bykov, R.S. Jakubek, S.A. Asher, Hydrophobic collapse initiates the poly(N -isopropylacrylamide) volume phase transition reaction coordinate, J. Phys. Chem. B 122 (2018) 3008–3014.
[34] D.M. Gray, A.R. Town, E. Niezabitowska, S.P. Rannard, T.O. McDonald, Dual-responsive degradable core-shell nanogels with tuneable aggregation behaviour, RSC Adv. 12 (2022) 2196–2206.
[35] I. Varga, A. Kardos, A. Borsos, T. Gilányi, Effect of internal charge distribution on the electrophoretic mobility of poly(N-isopropylacrylamide) based core-shell microgel particles, J. Mol. Liq. 302 (2020) 111979.
[36] B. Sierra-Martín, M.S. Romero-Cano, A. Fernández-Nieves, A. Fernández-Barbero, Thermal control over the electrophoresis of soft colloidal particles, Langmuir 22 (2006) 3586–3590.
[37] S.Z. Moghaddam, E. Thormann, The Hofmeister series: specific ion effects in aqueous polymer solutions, J. Colloid Interface Sci. 555 (2019) 615–635.
[38] S.Z. Moghaddam, E. Thormann, The Hofmeister series: specific ion effects in aqueous polymer solutions, J. Colloid Interface Sci. 555 (2019) 615–635.
[39] Y. Wu, S. Joseph, N.R. Aluru, Effect of cross-linking on the diffusion of water, ions, and small molecules in hydrogels, J. Phys. Chem. B 113 (2009) 3512–3520.
[40] William Bate Hardy, A preliminary investigation of the conditions which determine the stability of irreversible hydrosols, Royal Society 66 (1900) 424–433.
[41] G. Trefalt, I. Szilagyi, G. Téllez, M. Borkovec, Colloidal stability in asymmetric electrolytes: modifications of the schulze-hardy rule, Langmuir 33 (2017) 1695–1704.
[42] A. Chandra, S. Chowdhuri, Pressure effects on the dynamics and hydrogen bond properties of aqueous electrolyte solutions: the role of ion screening, J. Phys. Chem. B 106 (2002) 6779–6783.
[[43]] E.B. Zhulina, J.K. Wolterink, O.v. Borisov, Screening effects in a polyelectrolyte brush: self-consistent-field theory, Macromolecules 33 (2000) 4945–4953.
[44] T. Tadros, T. Tadros, Encyclopedia of Colloid and, Interface Science, 2013.
[45] A. Gupta, H.A. Stone, Electrical double layers: effects of asymmetry in electrolyte valence on steric effects, dielectric decrement, and ion-ion correlations, Langmuir 34 (2018) 11971–11985.
[46] D.M. Gray, A.R. Town, E. Niezabitowska, S.P. Rannard, T.O. McDonald, Dual-responsive degradable core-shell nanogels with tuneable aggregation behaviour, RSC Adv. 12 (2022) 2196–2206.
[47] A.R. Town, M. Giardiello, R. Gurjar, M. Siccardi, M.E. Briggs, R. Akhtar, T.O. McDonald, Dual-stimuli responsive injectable microgel/solid drug nanoparticle nanocomposites for release of poorly soluble drugs, Nanoscale 9 (2017) 6302–6314.
[48] A.R. Town, J. Taylor, K. Dawson, E. Niezabitowska, N.M. Elbaz, A. Corker, E. Garcia-Tuñón, T.O. McDonald, Tuning HIV drug release from a nanogel-based in situ forming implant by changing nanogel size, J. Mater. Chem. B 7 (2019) 373–383.
[49] B. Katana, D. Takács, A. Szerlauth, S. Sáringer, G. Varga, A. Jamnik, F.D. Bobbink, P.J. Dyson, I. Szilagyi, Aggregation of halloysite nanotubes in the presence of multivalent ions and ionic liquids, Langmuir 37 (2021) 11869–11879.
[50] P. Maity, B. Saha, G. Suresh Kumar, S. Karmakar, Effect of zwitterionic phospholipid on the interaction of cationic membranes with monovalent sodium salts, Langmuir, American Chemical Society (2018) 9810–9817.
[51] R. Tadmor, E. Hernández-Zapata, N. Chen, P. Pincus, J.N. Israelachvili, Debye length and double-layer forces in polyelectrolyte solutions, Macromolecules 35 (2002) 2380–2388.
[52] E. Niezabitowska, A.R. Town, B. Sabagh, M.D. Morales Moctezuma, V.R. Kearns, S.G. Spain, S.P. Rannard, T.O. Mcdonald, Insights into the internal structures of nanogels using a versatile asymmetric-flow field-flow fractionation method, Nanoscale Adv. 2 (2020) 4713–4721.
[53] Kielland Jacob, Individual activity coefficients of ions in aqueous solutions, J. Am. Chem. Soc. 59 (1937) 1675–1678.
[54] J.W. Polster, A.J. Souna, M.H. Motevaselian, R.A. Lucas, J.D. Tran, Z.S. Siwy, N.R. Aluru, J.T. Fourkas, The electrical-double layer revisited, Natural Sciences 2 (2022).
[55] S. Bhattacharjee, DLS and zeta potential - what they are and what they are not? J. Contr. Release 235 (2016) 337–351.
[56] A. Sze, D. Erickson, L. Ren, D. Li, Zeta-potential measurement using the Smoluchowski equation and the slope of the current-time relationship in electroosmotic flow, J. Colloid Interface Sci. 261 (2003) 402–410.
[57] M.M. Kohonen, M.E. Karaman, R.M. Pashley, Debye length in multivalent electrolyte solutions, Langmuir 16 (2000) 5749–5753.